Rodriguez Martinez, ED.; Bernal, SA.; Provis, JL.; Paya Bernabeu, JJ.; Monzó Balbuena, JM.; Borrachero Rosado, MV. (2013). Effect of nanosilica-based activators on the performance of an alkali-activated fly ash. Cement and Concrete Composites. 35(1):1-11. doi:10.1016/j.cemconcomp.2012.08.025.

Effect of nanosilica-based activators on the performance of an alkali-activated fly ash binder

Erich D. Rodríguez[1*], Susan A. Bernal[2†], John L. Provis[2†*], Jordi Paya[1], José M. Monzo[1], and María Victoria Borrachero[1*]

[1] *Instituto de Ciencia y Tecnología del Hormigón, Universitat Politècnica de València, 46022 Valencia, Spain*

[2] *Department of Chemical and Biomolecular Engineering, University of Melbourne, Victoria 3010, Australia*

[†] *Current address: Department of Materials Science and Engineering. University of Sheffield, Sheffield, United Kingdom.*

* To whom correspondence should be addressed. Email: errodnar@disca.upv.es, erichdavidrodriguez@gmail.com (EDR); j.provis@sheffield.ac.uk (JLP)

phone: +34-963 877 007 (75648), fax: +34-963 877 569

Con formato: Inglés (Estados Unidos)

Abstract

This paper assesses the effect of the use of an alternative activator based on nanosilica/MOH (M= K^+ or Na^+) blended solutions on the performance of alkali-activated fly ash binders. Binders produced with commercial silicate activators display a greater degree of reaction, associated with increased contents of geopolymer gel; however, mortars produced with the alternative nanosilica-based activators exhibited lower water demand and reduced permeability, independent of the alkali cation used. Na-based activators promote higher compressive strength compared with K-based activators, along with a refined pore structure, although K-activated samples exhibit reduced water demand. Zeolite type products are the major crystalline phases formed within these binders. A wider range of zeolites is formed when using commercial silicate solutions compared with the alternative activators. These results suggest that there are variations in the availability of Si in the system, and consequently in the alkalinity, depending on the silicate source in the activator, which is important in determining the nanostructure of the geopolymer gel.

Keywords: Alkali-activated binders, soluble silicate solutions, nanosilica, X-ray diffraction, scanning electron microscopy

1. Introduction

Interest in the development of alternative building materials such as alkali-activated binders has been promoted by the growth of the building industry, the increased performance requirements placed upon materials, and the higher sustainability criteria applied in construction. Alkali-activated binders represent an attractive alternative for the partial or complete substitution of Portland cement in the production of mortars and concretes, offering comparable performance and cost [1] while reducing greenhouse gas emissions [2]. Specifically, the alkali-activation of low calcium fly ashes (FA) has been extensively assessed over the past decades because these binders exhibit mechanical performance comparable to that reported for Portland cement, and because FA is an industrial by-product available worldwide. FA is produced in high amounts, especially in countries such as India and China, where an increased demand for cement is expected in the coming years. Despite the promising properties of these binders, and their ongoing commercialization, there are technological challenges associated with the variability of the raw materials from different sources, and the low sustainability of the current alkali-activators used [3].

In the activation of aluminosilicate precursors such as FA, the nature of the activator solution plays a key role in determining structural and mechanical performance. The most relevant characteristics related to the alkali activator are: the type of alkaline salt (usually silicate or hydroxide) [4-6]; the method of addition of the alkaline component (as a solution or in solid-state) [7-9], and the dosage of the alkali component, usually expressed as molar ratios considering the overall composition of the raw material. Additionally, it has been reported [4, 10-11] that the alkali cation supplied by the alkaline solution influences the first stages of binder formation, and consequently the mechanical performance of the final products. The alkali-activators conventionally used are sodium or potassium hydroxides, and/or sodium or potassium silicates [12]. Activation with K-containing solutions often leads to increased compressive strength development when compared with Na-containing solutions, where the size and charge density of the alkali cation play an important role in controlling the rate and extent of condensation during the polycondensation or crystallization process [13]. However, these effects are also dependent on the chemical and physical nature of the solid precursor used [5].

The embodied energy associated with the preparation of an alkali-activated binder is often estimated based on the contributions of the precursor and the alkaline activator. Some studies have analyzed the real energy consumed in fly ash based geopolymer production [14-15], identifying that the major contribution is associated with the type and concentration of the alkaline activator, and is between 0.5 MJ/t and 3.4 MJ/t. This is mainly related to the complex chemical processes required to manufacture these substances. For instance, the production of sodium silicate involves the calcination of sodium carbonate (Na_2CO_3) and quartz sand (SiO_2) at temperatures between 1400-1500ºC, producing large amounts of CO_2 as a secondary product [16-18]. This substantially increases the embodied energy of silicate-activated binders, reducing sustainability. However, sodium silicate ($Na_2O{\cdot}rSiO_2$, sometimes referred to as 'waterglass') is the activator which generally provides the highest compressive strength development at early ages of curing, and exhibits some technological advantages compared with other activators such as NaOH.

This then provides motivation for the examination of the current activators used in geopolymerization processes in terms of their sustainability, and the assessment of alternatives that can contribute to reducing the embodied energy of these binders. Some studies assessing alternative activators based on modified silica fume (MSF) have been conducted [19-21]. Likewise, agro-industrial wastes, as well as other silica sources, have been studied as alternative alkali-activators in order to obtain a more environmentally friendly alkali-activated binder with lower cost [22-27]. These results reveal that this alternative activator promotes similar or even better mechanical performance when compared with conventional activators.

Based on this background, the aim of this paper is to study alkali-activated low calcium fly ash binders, activated by chemically modified nanosilica. The effect of the alkali cation (Na^+ and K^+) on the structure of the binders is studied by X-ray diffraction (XRD), thermogravimetry and electron scanning microscopy (SEM/EDS). Compressive strength testing and mercury intrusion porosimetry (MIP) are conducted on mortar samples based on the binders produced, in order to generate a better understanding of the effect of the type of activator used, the gel structure formed, and the mechanical strength development of the materials.

2. Experimental program

2.1. Materials

The binders studied here were synthesized using a fly ash (FA) from Teruel Power Station in Andorra, Spain, with a specific gravity of 2520 kg/m^3 and a chemical composition as shown in Table 1. The FA was mechanically treated in a high impact mill (Mill2 Gabbrielli) to increase its reactivity. The particle size range determined by laser granulometry was 0.2-80 μm, with a mean particle size of 15 μm, and a specific surface of 1130 m^2/kg.

Table 1. Chemical composition of the fly ash from X-ray fluorescence analysis. LOI is loss on ignition at 950 ˚C

The X-ray diffraction pattern of the FA (Figure 1) shows that the major crystalline phases present are quartz (SiO_2; Powder Diffraction File (PDF) card # 00-046-1045), mullite ($Al_6Si_2O_{13}$; PDF# 00-015-0776), and Fe-rich phases such as hematite (Fe_2O_3; PDF# 00-033-0664), iron silicate (Fe_7SiO_{10}; PDF# 00-022-1118), and some ferrite spinels (magnetite - Fe_3O_4; PDF#00-019-0629, with and without substituent elements such as Mg and Al on both Fe^{2+} and Fe^{3+} sites). The presence of these phases is coherent with the high content of iron in the fly ash and has been previously observed in other fly ashes [28-30]. It is important to note that the ferrite spinels in the FA play an important role in the potential hosting of heavy metals, as Fe^{3+} sites can be substituted by trivalent cations such as Cr^{3+} [31].

Figure 1. Cu-K_α diffractogram of the fly ash after mechanical treatment

As alkali-activators, four alkaline solutions derived from hydroxide solutions and soluble silica sources were used. A commercial sodium silicate (SS) from Merck and a potassium silicate (SK) from IQE were used as reference soluble silica sources (Table 2). Two additional soluble silicates based on blends of a nanosilica suspension from H.S. Starck (L300, specific surface 300 m^2/g; Table 2) were also assessed. Alkali-activators were prepared by the dissolution of analytical sodium hydroxide (99 wt%) or potassium

hydroxide (85 wt%) pellets along with the silica source to obtain a molar oxide ratio SiO_2/M_2O equal to 1.16, where *M* corresponds to Na^+ or K^+.

Table 2. Chemical composition of reference silicate activators and nanosilica used to prepare nanosilica/MOH activators; data provided by the suppliers

2.2. Sample synthesis and test procedure

2.2.1. Pastes

Alkali-activator with a molar oxide ratio SiO_2/M_2O of 1.16 was incorporated at 12.0 wt% Na_2O or 18.2 wt% K_2O by mass of fly ash, providing equivalent alkali concentrations on a molar basis for the samples prepared with different alkalis. All specimens were produced by mechanical mixing for 4 minutes, including different contents of water in order to obtain similar workability (Table 3)**.** It is important to note that the water/binder values consider the liquids and solids contributed by both the activator and the precursor (i.e. binder = fly ash + anhydrous activator).

Table 3. Mix description of silicate-activated fly ash binders

For the structural study of hardened pastes, the specimens were cast in cylindrical molds and cured at a relative humidity (RH) of 90% and a temperature of 65ºC, for 48 h. Afterwards, samples were kept in a high humidity atmosphere (RH ≥ 90%) at room temperature (~25ºC). The reaction process was stopped at specified times by crushing the samples and submerging them in acetone for 15 min, filtering and drying. In order to prevent the carbonation of the powders thus obtained, these were stored in sealed containers, and then analyzed:

- X-ray diffraction (XRD) was carried out using a Bruker D8 Advance instrument with Cu Kα radiation and a nickel filter. The tests were conducted with a step size of 0.020º, for a 2θ range of 3º to 65º.
- A thermobalance TGA-850 (Mettler Toledo) was used to analyze crushed samples at a heating rate of 10ºC/min up to 1000ºC, with an alumina crucible in an dry air atmosphere.

- Scanning electron microscopy (SEM) was conducted using a JEOL JSM6300 microscope with a tungsten filament electron source, and 20kV accelerating voltage. The samples were evaluated in high vacuum mode. Attached to this instrument a Link-Isis (Oxford Instruments) X-ray spectrometer system (energy dispersive spectroscopy (EDS)) was used to determine the chemical compositions of the phases identified.

2.2.2. Mortars

Mortars were produced using a siliceous sand with a fineness modulus of 4.1 and specific weight of 2680 kg/m^3, in accordance with the standard procedure UNE-EN 196-12005. All samples were formulated with a standard fly ash:sand ratio of 1:3, cast in prismatic moulds of 40×40×160 mm, compacted and mechanically vibrated for three minutes. Curing was conducted in similar conditions as previously described for pastes; however, after the period of curing at high temperature, mortars were stored in sealed containers at RH ~90% and room temperature until testing. Compressive strength was determined after 2, 28 and 60 days following the standard testing protocol UNE-EN-1015-11. Additionally, mercury intrusion porosimetry (MIP) was conducted after 28 days using an AutoPore IV 9500 (Micromeritics) instrument, with applied intrusion pressures between 13.8 kPa and 227.4 MPa.

3. Results and discussion

3.1. Water demand

From visual inspection, it was possible to identify that mixes produced with reference K-based activators (commercial potassium silicate solution) exhibited increased workability when compared with pastes produced with the reference Na-based activator (commercial sodium silicate solution), which allowed a significant reduction of the total water included in these binders while achieving a similar slump. Similar behavior has been reported in the literature [5] for pastes prepared with K-based activators, which exhibit increased slump compared to those prepared with Na-based activators. Additionally, the lower silica content of the K-containing solutions will also have an effect in the fresh mixes, because an increased content of silica in the alkali activator (higher Ms) causes reduced workability of the fresh mixture, related to the higher viscosity identified in both Na and K silicate solutions at increased silica concentrations [12].

The water demand of the binders prepared with the nanosilica-based activator is lower than that of the pastes based on the reference silicate activators. Pastes including the nanosilica-solution presented better workability than those prepared with commercial silicate activator, independent of the alkali cation included in the solution, at an equivalent M_2O/SiO_2 molar ratio. This is a consequence of the structural differences between the nanosilica activator and the commercial silicate solutions. The low water demand of the L300-K paste is particularly notable, where a water content less than half of that of the S-Na sample is sufficient to provide good workability.

It is expected that in the commercial silicate solutions there will be a wide range of dissolved silicate species, and among these, increased oligomer sizes affect the kinetics of the exchange of silicate units during geopolymerization [32], contributing to an increment in the viscosity of the solution, and consequently to the reduced workability of the activated pastes. Conversely, in the nanosilica-derived activator, the rate of release of soluble silicates is affected by the degree of dissolution of the particles in the hydroxide solutions during the preparation of the activator. Considering that the time of preparation of the activator is not longer than 5 hours before use (sufficient time for the solution to cool to room temperature after the exothermic dissolution), not all of the nanosilica will be completely dissolved in the hydroxide solution, and the oligomers formed in these silicates might be lower in size compared to those in commercial silicates. This would then decrease the viscosity of the nanosilica-derived activators, and consequently contribute to the higher workability of the pastes produced with this activator, with reduced water demand.

Improved workability associated with lower water demand in these binders is desirable from a durability point of view, because a reduced degree of permeability of aggressive agents through the hardened binders might be able to be achieved using these alternative activators to enable the use of lower water/binder ratios. Detailed analysis of the pore structure of these systems is presented later in this paper.

3.2. Compressive strength

All of the binders assessed show compressive strengths between 84 and 88 MPa after 2 days of curing at 65˚C (Figure 2). These mortar compressive strength values enable the classification of these materials as high performance binders, considering that conventional Portland cement concretes with compressive strengths up to 60 MPa are classified as high performance, and to achieve these strengths generally requires the addition of chemical and/or mineral admixtures [33].

Figure 2. Compressive strength of alkali-activated fly ash mortars, as a function of the nature of the activator. Error bars indicate one standard deviation either side of the mean

As a consequence of the wide range of factors affecting the mechanical strengths of fly ash geopolymer binders, and the physical and chemical differences between fly ash and activator sources used by different research teams, it is difficult to make direct comparisons between the strengths reported by different authors. However, considering the relationship between the molar composition of the precursor and the mechanical strength proposed by Duxson and Provis [34], this ash will be expected to give good strength based on its chemical composition, which is coherent with the results reported here.

Mortars produced with Na-based activators present higher compressive strength than those with K-based activators. In both cases, slightly higher compressive strengths are obtained when using commercial silicates, especially at early ages. This effect is more notable in samples activated with the L300-K solution, which present compressive strengths up to 10MPa lower than the reference specimens (S-K). However, specimens prepared with the modified nanosilica activators present a clear linear trend in the strength development, so that at longer periods of curing (60 days) the compressive strengths of these mortars are comparable to those reported for the reference samples (S-Na and S-K).

These results are coherent with the mechanisms of activation which are known to take place when different alkali cations are incorporated in the binder. Xu *et al.* [35] observed that activation with NaOH promotes a higher degree of dissolution of aluminosilicate solids when compared with KOH. This is attributed to the higher capacity of NaOH to

favor the release of silicate and aluminate monomers [36-37], while K promotes condensation reactions to a greater extent, leading to the presence of more polysilicate species [13].

In alkali activation of metakaolin, the rate of reaction in alkaline K-enriched environments is sufficient to promote a high extent of dissolution while favoring condensation of reaction products at early ages [37]. This is one of the main reasons why, in metakaolin-based geopolymers, increased compressive strengths are obtained using K silicate activators compared with systems where Na silicate is the alkali source. Considering that the rate of dissolution of fly ash in an alkaline environment is lower than that of metakaolin [34], it might be expected that there would be a retardation of reaction kinetics when using K-based activators. This is consistent with the lower compressive strength development exhibited by S-K and L300-K samples. The slightly lower mechanical strength values at early ages of curing reported for mortars prepared with the modified nanosilica can be attributed to the lower dissolved silica content of the nanosilica/MOH solutions compared with commercial silicate solutions, where the presence of remnant, partially dissolved silica particles slows down the availability of SiO_2 in the system.

3.3. Pore size distribution

The MIP technique has some limitations related to measuring pore parameters in cementitious materials due to the presence of different sizes and shapes of pores, where deviations from cylindrical pore shapes will increase the measured volume of the very small pores [38]. However, it is still a valuable technique providing information about the threshold diameters and intrudable pore space, giving a better understanding of the effects of the different activators on the connectivity and capacity of the pore structure in the geopolymers assessed.

In general, K-geopolymers present lower total porosity than Na-geopolymer mortars, as seen by the lower cumulative volume intruded (Figure 3). Also, the lowest porosity is exhibited by samples prepared with the chemically modified nanosilica activator. Mortars produced with the K-nanosilica activator (L300-K) reported a total porosity of 6.32%, followed by those specimens produced with the Na-nanosilica activator (L300-Na) with a total porosity of 9.75%. These results are consistent with the reduced water demand of the

chemically modified nanosilica-activated geopolymers, highlighting the benefit of using this alternative activator.

Figure 3. Cumulative volume of mercury intruded as a function of pore diameter for S-Na, L300-Na and L300-K mortars after 28 days of curing

The pore size distributions of the mortars assessed are presented in Figure 4, as calculated from the applied pressure via the Washburn equation [39], assuming a contact angle of 130.0 degrees. In general, only slight differences are identified between the samples in terms of the volumes of pores with diameters higher than ~10μm in samples prepared with different alkali cations, despite the reduced water demand exhibited by K-activated geopolymers compared with the Na-activated geopolymer mortars.

Figure 4. Pore size distributions obtained from mercury intrusion data for silicate-activated fly ash mortars with 28 days of curing

A remarkable effect of the alkali cation on the pore size distribution is identified in the region of diameters smaller than 1 μm, where an increased pore volume is reported for L300-Na mortars compared with L300-K mortars. In this region two types of porosity can be identified: macropores (50-200 nm) and mesopores (3.6-50nm). Mesopores are present into the aluminosilicate gel network due to short-range ordering which is characteristic of an amorphous material. Macropores are formed during the early stages of geopolymerization, and may transform to mesopores with the progress of the polycondensation of hydrated gels in the binders, as a consequence of the filling of the larger pores with the new reaction products, particularly given the relatively high Ca content of the fly ash used here. On the other hand, pores larger than 200nm in the geopolymer pastes are likely to be associated with the interfacial spaces between partially-reacted or unreacted fly ash particles and the geopolymer gel [38, 40]. It is important to note that complete dissolution and reaction of precursors have never been observed in fly ash geopolymer binders, in particular when the solid precursor contains unreactive crystalline phases as is the case for the precursor used in the present study (Figure 1).

These results indicate that, although L300-Na mortars have higher water content and thus report a higher total porosity than L300-K mortars, a higher extent of polycondensation of

339 the geopolymer gel is taking place in the presence of Na. This leads to the refinement of
340 the pore network, which contributes to the increased compressive strength. The presence
341 of pores of smaller diameter is important from a durability point of view, considering that
342 the diffusion of aggressive agents into the binders usually takes place through the larger
343 pores.
344
345 ***3.4. X-ray diffraction***
346
347 In samples prepared with Na-based activators, the major crystalline phases previously
348 identified in the unreacted fly ash (Figure 1) are again observed; the crystalline
349 components of the fly ash are un-reactive. In pastes activated with commercial sodium
350 silicate, the main crystalline reaction products identified correspond to a calcium silicate
351 hydrate containing some sodium (N-C-S-H in cement chemistry terminology)
352 ($Na_2Ca_2Si_2O_7 \cdot H_2O$; PDF# 00-022-0891), analcime ($NaAlSi_2O_6 \cdot H_2O$); PDF# 00-002-
353 0417), gismondine ($(Ca,Na_2)Al_2Si_2O_8 \cdot 4H_2O$; PDF# 00-021-0840), Na-P1 zeolite
354 ($Na_2Al_2Si_2O_8 \cdot xH_2O$; PDF# 00-0025-0777) which is also a gismondine type structure,
355 along with the zeolites gonnardite ($(Na,Ca)_2(Si,Al)_5O_{10} \cdot 2H_2O$; PDF# 00-042-1381) and
356 mesolite ($Na_2Ca_2Al_5Si_9O_{30} \cdot 8H_2O$; PDF# 00-024-1064), which both present the natrolite
357 type structure. When activating with L300-Na, the Na-P1, analcime and N-C-S-H are not
358 identified; however, a new zeolite structure corresponding to faujasite
359 ($Na_2Al_2Si_{3.3}O_{10.6} \cdot 7H_2O$) (PDF# 00-012-0228) is detected. These zeolites have been also
360 formed in other fly ash geopolymer systems [41, 42] and through the hydrothermal
361 production of zeolites using a similar fly ash precursor [43, 44].
362
363 **Figure 5**. Cu-K_α diffractograms of the fly ash activated with Na-based activators. Peaks
364 present in both diffractograms are labeled in only one diffractogram for visual clarity.
365
366 The crystallization of zeolites from amorphous aluminosilicates is determined by the
367 dissolution rate of the precursor, which is controlled by at least two processes: (1) the
368 breakage of surface bonds due to the action of solvent and formation of soluble species
369 that leave the surface of the dissolving solid (directly proportional to the external surface
370 area), and (2) the reaction of the soluble species from the liquid phase on/with the surface
371 of the dissolving solid (depending only indirectly on the concentration of NaOH via the
372 change of the concentrations of reactive silicate and aluminate species in the liquid phase)

[34, 45]. Considering that all of the samples have been prepared with the same fly ash precursor, it is likely that the structural differences are associated with variations in the alkalinity provided by the different silicate activators.

In the hydrothermal preparation of pure analcime from pure silica and alumina sources at intermediate alkalinity conditions, the Na-P1 zeolite has been identified in the early stages of reaction, and it then exhibits a gradual dissolution while the crystallization of analcime is taking place; however, increasing the alkalinity in the system favors the formation of faujasite instead of Na-P1 or analcime [46]. Using the commercial silicates here, the coexistence of analcime and Na-P1 zeolites is achieved, along with the formation of a wide range of zeolites. This indicates that the activation conditions promoted by this activator are favoring the nucleation and growth of stable crystalline zeolites. Conversely, using the NaOH/nanosilica derived activator leads to a lower availability of SiO_2 species in the systems, which is likely to maintain a higher alkalinity compared with commercial silicate solutions at the early times of reaction, consequently promoting the formation of faujasite.

Hajimohammadi et al. [47] studied geopolymer formation from systems with separate Si and Al sources, and observed that analcime formation occurred in systems with low Si availability, while faujasite development was promoted at intermediate or high rates of high Si availability. This differs from the trends observed here, where reversed results are obtained, indicating that the mechanisms of gel and zeolite nucleation and growth in binders where Si and Al sources are separated differ from those where Si and Al are provided in parallel by an aluminosilicate precursor (e.g. fly ash) along with an external source of Si (activator). Considering that analcime is a relatively high-silica zeolite and its formation is likely to occur in areas enriched in Si, it seems that the additional Si species contributed by a highly dissolved activator can favor the formation of this phase when using the commercial sodium silicate.

The use of commercial potassium silicate (S-K) (Figure 6) as activator also promotes the formation of crystalline reaction products, such as lithosite ($K_3HAl_2Si_4O_{13}$; PDF# 00-037-0457), K-cymrite ($KAlSi_3O_8 \cdot H_2O$; PDF# 00-016-0385) and aluminosilicate zeolites with a chabazite-K type structure ($K_{10.9}Al_{11.1}O_{72}Si_{24.9} \cdot 25H_2O$; PDF# 00-037-0792). K-cymrite is also identified in binders prepared with the L300-K activator, along with hydrodelhayelite

407 ($KCa_2(Si_7Al)O_{17}(OH)_2.6H2O$; PDF# 00-041-0611), and a chabazite-K zeolite
408 ($KAlSiO_4.xH_2O$; PDF# 00-053-1777). The formation of zeolite-like products including
409 calcium (in particular hydrodelhayelite; chabazite is also known to show Ca substitution,
410 although this was not explicitly observable here) is likely to be related to the weaker
411 zeolite structure forming tendencies of potassium here compared to sodium in Figure 5;
412 pure sodium zeolites form reasonably readily, while pure potassium zeolites are less
413 common, which leads to the formation of mixed-cation species as identified here.
414
415 **Figure 6**. Cu-K_α diffractograms of the fly ash activated with K-based activators. Peaks
416 present in both diffractograms are labeled in only one diffractogram for visual clarity.
417
418 ***3.5. Thermogravimetry***
419
420 The thermograms of the binders (Figure 7) after 28 days of curing exhibit an onset of
421 weight loss at temperatures lower than 300ºC, which is associated with the physically
422 bound and zeolitic water present in the reaction products (dominated by an aluminosilicate
423 type-gel) which can be easily removed from the sodium/potassium silicate gel surface at
424 these temperatures [48-50]. Loss of weight at temperatures higher than 300ºC is
425 consistent with dehydroxylation by condensation of the bound silanol groups, which is
426 completed at 500ºC [48].
427
428 **Figure 7.** Thermograms of silicate-activated fly-ash binders at 28 days of curing
429
430 Differences in the total weight loss are identified between samples with nanosilica-based
431 activators and commercial silicate activators. This is more marked when comparing
432 samples with different alkali cations, where geopolymers activated by Na salts presented a
433 total weight loss of ~13% while K-geopolymers presented ~11% weight loss. This is
434 consistent with the structural differences in the binders as identified by MIP and XRD as
435 discussed above. The total loss of weight in K-activated geopolymer paste is 18% lower
436 than in the Na-activated specimens, which is consistent with the difference in water
437 content between the samples. However, some of the additional weight loss reported for
438 Na-activated binders may also be attributed to a larger content of gel reaction products
439 having been formed at the time of curing at which these samples were assessed, compared
440 with K-activated samples. This is consistent with the higher compressive strength and

reduced permeability reported for Na-activated samples, independent of the silica source in the activator.

Differential thermogravimetric curves (DTG; Figure 8) show a broad peak from room temperature up to ~300ºC in all samples. The main peak identified in both S-Na and L300-Na geopolymers presents a minimum at ~103ºC, attributed to the freely evaporable water present in large pores in the geopolymer gel. The increased intensity of this peak in samples activated with the commercial silicate solutions indicates a higher extent of aluminosilicate gel formation, coherent with the high compressive strength identified in mortars prepared with this binder. It is important to note that the first minimum related to the loss of weight of evaporable water in these fly ash geopolymers (~103ºC) is at a higher temperature than that which has been reported for metakaolin geopolymers (~58ºC) with comparable formulations [50], indicating that the use of FA as a precursor for the production of these binders favors the formation of denser geopolymer gels with tightly absorbed water in small pores, or as condensed hydroxyl groups on the surface of the gel [48, 51].

Figure 8. Differential thermograms of silicate-activated fly ash

In the samples S-Na and S-K a second peak is also observed at ~141ºC. In MK-based geopolymers and activated MK/GBFS blends the presence of this second peak has been associated with the dehydration of the zeolite-type product (hydroxysodalite in that case) formed along with the geopolymer gel [50]. Oh et al. [52] reported that the geopolymer gel formed through the alkali-activation of fly ash presents a disordered form of the ABC-6 family of zeolitic products, which contains different polytypes such as chabazite, and ranging from amorphous structure to polycrystalline in the case of high alkalinity mixes.

Crystalline chabazite has previously been reported as a zeolitic product in sodium-fly ash geopolymer systems [41]; however, crystalline chabazite structures are observed here exclusively in samples with K-based activators (Figure 6). Weight loss of chabazite-type zeolites has been reported at temperatures of 162ºC for chabazite-Na ("herschelite"), and 192°C for chabazite-K [53, 54], which probably indicates that the second peak identified in DTG analysis of these binders (Figure 8) is likely to be related to geopolymer gel with a chabazite-like nanostructure. A higher intensity of this peak is shown for pastes activated

475 with commercial silicates, which can be associated with the larger degree of reaction and
476 increased ordering of the gels formed.
477
478 A third peak at ~596ºC is only observed in commercial-silicate activated geopolymers (S-
479 Na and S-K), and is attributed to the complete dehydroxylation of zeolites present in the
480 binder. Conversely, a weaker signal at 509ºC, and a small and poorly defined peak at
481 490ºC are identified in L300-Na and L300-K binders respectively. The shifting of the
482 dehydroxylation peak towards lower temperatures is associated with lower alkali and Al
483 content, because of the greater strength of the bond between the water and the Na^+ or K^+
484 cations in this case [55, 56].
485
486 A low intensity peak at ~847ºC is identified in L300-K, corresponding to decomposition
487 of the carbonates, probably sodium or potassium carbonate (Figure 6). Similar peaks
488 (~780-800ºC) with reduced intensity are also exhibited by S-Na and S-K geopolymers.
489
490
491 ***3.6. Scanning electron microscopy (SEM/EDS)***
492
493 Fly ash geopolymers activated with commercial sodium silicate (Figure 9) exhibit a
494 heterogeneous gel structure, with embedded particles of varying morphologies (Figure
495 9A): smooth spherical particles (Figure 9B), agglomerations of rectangular crystalline
496 particles mostly composed of Al and Si (Figure 9C) surrounded by an Si-rich gel,
497 spherical units formed from the agglomeration of tubular particles enriched in Fe (Figure
498 9D), and crystalline particles with a dendritic-type structure with a high content of Fe and
499 containing similar proportions of Al and Si (Figure 9E). Hollow cavities with spherical
500 shape are associated with the partial dissolution of fly ash particles during the
501 geopolymerization reaction, where the un-reacted remnant fly ash particles are not bound
502 to the geopolymer gel, and fall out from their positions in the cavities during sample
503 preparation for microscopic analysis.
504
505 In analysis of fly ashes from different sources [57], it has been identified that this material
506 presents a spherical particle shape, mostly consisting of amorphous aluminosilicate, along
507 with iron-rich spheres composed of iron oxide mixed with amorphous aluminosilicate with
508 variations in the contents of Al, Si and Fe. Specifically, the ferrospheres in fly ash present

509 a microstructure that can include smooth, polygonal, dendritic, granular and molten drop
510 characteristics [58], and can often be represented as a nanocomposite with ‘‘core–shell”
511 structure, where the core is formed from spinel, hematite and quartz crystals (phases
512 observed by XRD in the fly ash used here), and the shell consists of glasses [59].
513
514 Considering the chemical compositions of the different phases forming the geopolymer
515 and the microstructural characteristics reported for unreacted fly ash, it is inferred that the
516 smooth spherical particles correspond to undissolved FA, while the agglomerated
517 rectangular particles are identifiable according to their composition as being mullite, and
518 those with dendritic-type structure are likely to be associated with the ferrite spinels
519 previously observed by XRD (Figure 5). This is coherent with the observations made by
520 Lloyd et al. [60] who identified remnant particles of un-reacted fly ash, along with
521 crystalline phases such as mullite, in fly ash-based geopolymers. This is attributed to the
522 differential solubilities of the phases composing the fly ash under the activation conditions
523 used, especially where those presenting high crystallinity are less soluble. In the fly ash
524 assessed, mullite has been identified by XRD, and is likely to be responsible for the
525 particles identified in Figure 9C.
526
527 **Figure 9.** Scanning electron micrographs and corresponding EDS spectra of the binder
528 activated with a commercial sodium silicate (S-Na)
529
530 Binders activated with the NaOH/nanosilica derived activator (Figure 10) present only
531 slight microstructural differences compared with commercial Na-silicate activated pastes.
532 In this case, it is also possible to identify a partially dissolved fly ash particle with a
533 needle-like phase over its surface (Figure 10B), which is rich in Al and Si. This phase is
534 likely to be associated with mullite crystals, including some Fe substituting for Al in the
535 mullite structure [61].
536
537 **Figure 10.** Scanning electron micrographs and corresponding EDS spectra for the binder
538 activated with NaOH/nanosilica-derived activator (L300-Na)
539
540 Dendritic type particles assigned to the ferrite spinels forming the unreacted FA are also
541 identified (Figure 10C), which is coherent with XRD (Figure 5). This is consistent with
542 the observations of Lloyd et al. [60] who observed that iron-rich phases in a fly ash

precursor are relatively unreactive. In this binder, a Ca- and Si-rich needle-like morphology is visible inside one of the hollow cavities, presenting some traces of Na and low contents of Al. Taking this into account, this morphology can be associated with some sort of C-S-H phase. It is important to note that XRD results do not reveal the formation of a long range-ordered C-S-H when using this activator; these phases are therefore identifiable as showing at most short-range order.

The geopolymer gel embedding the different particles presents similar chemical composition, independent of the silicate source, using Na-based activators. However, it seems that there is a higher degree of interaction between this gel and the fly ash particles in the binders prepared with the nanosilica-derived activator. This is coherent with the reduced permeability exhibited by this binder (Figure 3), providing further evidence of the effectiveness of using this alternative activator for producing geopolymers.

Binders prepared with a commercial K-silicate activator (Figure 11) also show mullite crystals which were originally embedded within fly ash particles. As the reaction progressed, the glass phase dissolved and exposed the mullite needles. Similarities in the chemical composition of the geopolymer gel formed are again identified between the samples which used the commercial K-silicate activator (Figure 11A) and the KOH/nanosilicate derived activator (Figure 11B).

Figure 11. Scanning electron micrographs, and corresponding EDS spectra, of the binders activated with (A) commercial potassium silicate solution (S-K) and (B) KOH/nanosilica derived activator

4. Conclusions

The production of high mechanical strength and low permeability geopolymers has been achieved using alternative activators based on modified nanosilica. These binders show an extent of reaction which is slightly lower than that of binders produced from the same fly ash using commercial sodium silicate activators, but mechanical strengths are similar. The water demand and porosity of the samples prepared with the nanosilica-based activators are lower than for the case of the commercial silicate activators, which is attributed to the slightly delayed release of silica from the solid nanosilica particles, which remain in

suspension in the solution during the early ages of reaction and then release silica later in the reaction process. The crystalline zeolite phases formed in the samples differ slightly between the nanosilica-derived and traditional activators, again consistent with the differences in silica release rates from the two activators. Microstructural analysis shows that the geopolymer gel is more tightly bound to the partially reacted fly ash particles in the case of the nanosilica-derived activator, consistent with the reduced porosity of these binders. The use of the nanosilica activator may also bring advantages in terms of the environmental profile of the materials.

Acknowledgements

This study was sponsored by the *Ministerio de Ciencia e Innovación* of Spain (Project GEORES MAT2010-19934 and research scholarship BES-2008-002440), European regional development fund (FEDER), and the *Universitat Politècnica de València* (Spain). The participation of SAB and JLP was funded by the Australian Research Council (ARC), including partial funding through the Particulate Fluids Processing Centre, a Special Research Centre of the ARC. A special acknowledgement is also due to the Centre of Electron Microscopy of the *Universitat Politècnica de València* and Pedro Garcés from the *Universidad de Alicante* for support in some experiments.

References

1. Duxson P., Fernández-Jiménez A., Provis J.L., Lukey G.C., Palomo A., van Deventer J.S.J. Geopolymer technology: the current state of the art. J Mater Sci 2007, 42(9): 2917-2933.
2. Duxson P., Provis J.L., Lukey G.C., van Deventer J.S.J. The role of inorganic polymer technology in the development of green concrete. Cem Concr Res 2007, 37(12): 1590-1597.
3. van Deventer J.S.J., Provis J.L., Duxson P., Brice D.G. Chemical research and climate change as drivers in the commercial adoption of alkali activated materials. Waste Biomass Valor 2010, 1(1):145-155.
4. van Jaarsveld J.G.S., van Deventer J.S.J. Effect of the alkali metal activator on the properties of fly ash-based geopolymers. Ind Eng Chem Res, 1999, 38(10):3932-3941,

611 5. Phair J.W., van Deventer J.S.J. Effect of silicate activator pH on the leaching and
612 material characteristics of waste-based inorganic polymers. Miner Eng 2001,
613 14(3):289–304.
614 6. Fernández-Jiménez A., Palomo A. Composition and microstructure of alkali activated
615 fly ash binder: Effect of the activator. Cem Concr Res 2005, 35:1984 – 1992
616 7. Yang K.-H., Song J.-K., Ashour A.F., Lee E.-T. Properties of cementless mortars
617 activated by sodium silicate. Constr Build Mater 2008, 22(9):1981-1989.
618 8. Yang K.-H., Song J.-K. Workability loss and compressive strength development of
619 cementless mortars activated by combination of sodium silicate and sodium
620 hydroxide. J Mater Civ Eng 2009, 21: 119-127
621 9. Hajimohammadi A., Provis J.L., van Deventer J.S.J. One-part geopolymer mixes from
622 geothermal silica and sodium aluminate. Ind Eng Chem Res. 2009, 47(23): 9396-
623 9405.
624 10. Duxson P., Mallicoat S.W., Lukey G.C., Kriven W.M., van Deventer J.S.J. The effect
625 of alkali and Si/Al ratio on the development of mechanical properties of metakaolin-
626 based geopolymers. Colloids Surf A 2007, 292(1): 8-20.
627 11. Fernández-Jiménez A., Palomo A., Criado M. Alkali activated fly ash binders. A
628 comparative study between sodium and potassium activators. Mater Constr. 2006,
629 56(281): 51-56.
630 12. Provis, J.L. Activating solution chemistry for geopolymers. In: Provis J.L., van
631 Deventer, J.S.J. (editors.) Geopolymers: Structures, Processing, Properties and
632 Industrial Applications, Woodhead Publishing, Abingdon UK, 2009, p50-71.
633 13. McCormick A.V., Bell A.T. The solution chemistry of zeolite precursors. Catal Rev
634 Sci Eng 1989, 31: 97-127.
635 14. Witherspoon R., Wang H., Aravinthan T., Omar T. Energy and emissions analysis of
636 fly ash based geopolymers. Proceedings of SSEE 2009 International Conference.
637 Melbourne, Australia, 2009.
638 15. Tempest B., Sanusi O., Gergely J., Ogunro V., Weggel D. Compressive strength and
639 embodied energy optimization of fly ash based geopolymer concrete. Proceedings of
640 the 2009 World of Coal Ash (WOCA) conference. Lexington, KY, USA, 2009.
641 16. McLellan B.C., Williams R.P., Lay J., van Riessen A., Corder G.D. Costs and carbon
642 emissions for geopolymer pastes in comparison to ordinary Portland cement. J
643 Cleaner Prod 2011, 19: 1080-1090.

644 17. Deabriges J. Process for the manufacture of sodium silicate. United States Patent
645 4,336,235, 1982.
646 18. Fawer M., Concannon M., Rieber W. Life cycle inventories for the production of
647 sodium silicates. Int J Life Cycle Assess 1999, 4(4): 207-212.
648 19. Živica V. High effective silica fume alkali activator. Bull Mater Sci 2004, 27(2): 179–
649 182.
650 20. Živica V. Effectiveness of new silica fume alkali activator. Cem Concr Compos 2006.
651 28(1): 21–25.
652 21. Rouseková I., Bajza A., Živica V. Silica fume-basic blast furnace slag systems
653 activated by an alkali silica fume activator. Cem Concr Res 1997, 27(12): 1825-182
654 22. Rodríguez E. Effect of Si/Al/Na/Ca ratio in geopolymeric materials based on
655 metakaolin. Master Thesis. Universidad del Valle. Cali, Colombia. 2008.
656 23. Rodríguez E. Effectiveness of alkali-activators based on different sources of silica for
657 the manufacture of fly ash geopolymer systems. Master Thesis. Universidad
658 Politécnica de Valencia, Spain. 2009.
659 24. Detphan S., Chindaprasirt P. Preparation of fly ash and rice husk ash geopolymer. Int
660 J Miner Metall Mater 2009, 16(6): 720-126.
661 25. Songpiriyakij S., Kubprasit T., Jaturapitakkul Ch., Chindaprasirt P. Compressive
662 strength and degree of reaction of biomass and fly ash-based geopolymer. Constr
663 Build Mater 2010, 24(3): 236-240.
664 26. Bernal S.A., Rodríguez E.D., Mejía de Gutiérrez R., Provis J.L., Delvasto S.
665 Activation of metakaolin/slag blends using alkaline solutions based on chemically
666 modified silica fume and rice husk ash. Waste Biomass Valor 2012, 3(1): 99-108.
667 27. Wongpa J., Kiattikomol K., Jaturapitakkul C., Chindaprasirt P. Compressive strength,
668 modulus of elasticity, and water permeability of inorganic polymer concrete. Mater
669 Des 2010, 31: 4748-4754.
670 28. Winburn R.S., Lerach S.L., McCarthy G.J., Grier D.G., Cathcart J.D. Quantification
671 of ferrite spinel and hematite in fly ash magnetically enriched fractions. Adv X-Ray
672 Anal 2000, 43: 350-355.
673 29. Vassileva S.V., Menendez R., Alvarez D., Diaz-Somoano M., Martinez-Tarazona
674 M.R. Phase-mineral and chemical composition of coal fly ashes as a basis for their
675 multicomponent utilization. 1. Characterization of feed coals and fly ashes. Fuel 2003,
676 82:1793–181

30. Williams R.P., van Riessen A. Determination of the reactive component of fly ashes for geopolymer production using XRF and XRD. Fuel 2010, 89(12): 3683-3692.
31. Provis J.L., Rose V., Bernal S.A., van Deventer J.S.J. High-resolution nanoprobe X-ray fluorescence characterization of heterogeneous calcium and heavy metal distributions in alkali-activated fly ash. Langmuir 2009, 25(19): 11897–11904
32. Bahlmann E.K.F., Harris R.K., Rockliffe J.W., Smith E.G. Silicon-29 NMR self-diffusion and chemical-exchange studies of concentrated sodium silicate solutions. J Chem Soc, Faraday Trans. 1997, 93: 93-98.
33. Hewlett P.C. Lea's Chemistry of Cement and Concrete, 4th Ed. Elsevier, Oxford, UK, 1998
34. Duxson P., Provis J.L. Designing precursors for geopolymer cements. J Am Ceram Soc 2008. 91(12): 3864-3869.
35. Xu, H., van Deventer, J.S.J., Lukey, G.C. Effect of alkali metals on the preferential geopolymerization of stilbite/kaolinite mixtures. Ind Eng Chem Res 2001, 40(17): 3749-3756.
36. Duxson P., Lukey G.C., Separovic F., van Deventer J.S.J. Effect of alkali cations on aluminium incorporation in geopolymeric gels. Ind Eng Chem Res 2005, 44(4): 832-839.
37. Duxson P., Provis J.L., Lukey G.C., van Deventer J.S.J., Separovic F., Gan Z.H. ^{39}K NMR of free potassium in geopolymers. Ind Eng Chem Res 2006. 45(26): 9208-9210.
38. Diamond S. Mercury porosimetry. An inappropriate method for the measurement of pore size distribution in cement-based materials. Cem Concr Res 2000, 30: 1517-1525.
39. Washburn E.W. Note on method of determining the distribution of pore sizes in porous materials. Proc Nat Acad Sci U.S.A. 1921, 7(4): 115-116.
40. Kovalchuk G., Fernández-Jiménez A., Palomo A. Alkali-activated fly ash: Effect of thermal curing conditions on mechanical and microstructural development – Part II. Fuel 2007, 86: 315-322
41. Criado M., Fernández-Jiménez A., de la Torre A.G., Aranda M.A.G., Palomo A. An XRD study of the effect of the SiO_2/Na_2O ratio on the alkali activation of fly ash. Cem Concr Res 2007, 37: 671-679
42. Lloyd R.R. Accelerated ageing of geopolymers. In: Provis J.L, van Deventer, J.S.J. (Eds.) *Geopolymers: Structures, Processing, Properties and Industrial Applications*, Woodhead Publishing, Abingdon UK. 2009, p. 139-166.

711 43. Querol X., Alastuey A., Fernández-Turiel J.L., López-Soler A. Synthesis of zeolites
712 by alkaline activation of ferro-aluminous fly ash. Fuel 1995, 74(8): 1226-1231.
713 44. Querol X., Plana F., Alastuey A., López-Soler A. Synthesis of Na-zeolites from fly
714 ash. Fuel 1997, 76(8): 793-799.
715 45. Antonić T., Čižmek A., Subotić B. Dissolution of amorphous aluminosilicate zeolite
716 precursors in alkaline solutions: Part 2.- Mechanism of the dissolution. J Chem Soc
717 Faraday Trans 1994, 90(13): 1973-1977.
718 46. Kohoutková M., Kloužkova A., Maixner J., Mrázová M. Preparation and
719 characterization of analcime powders by X-ray and SEM analysis. Ceram–Silik 2007,
720 51(1): 9-14.
721 47. Hajimohammadi A., Provis J.L., van Deventer J.S.J. The effect of silica availability
722 on the mechanism of geopolymerisation. Cem Concr Res 2011, 41(3): 210-216.
723 48. Duxson P., Lukey G.C., van Deventer J.S.J. The thermal evolution of metakaolin
724 geopolymers: Part 1 – Physical evolution. J Non-Cryst Solids 2006, 352:5541-5555.
725 49. Duxson P., Lukey G.C., van Deventer J.S.J. The thermal evolution of metakaolin
726 geopolymers: Part 2 – Phase stability and structural development. J Non-Cryst Solids
727 2007, 353:2186-2200.
728 50. Bernal S.A., Rodríguez E.D., Mejía de Gutiérrez R., Gordillo M., Provis J.L.
729 Mechanical and thermal characterization of geopolymers based on silicate-activated
730 metakaolin/slag blends J Mater Sci. 2011, 46(16): 5477-5486.
731 51. Duxson P., Lukey G.C., van Deventer J.S.J. Physical evolution of Na-geopolymer
732 derived from metakaolin up to 1000˚C. J Mater Sci 2007, 42:3044-3054.
733 52. Oh J.E., Monteiro P.J.M., Jun S.S., Choi S., Clark S.M. The evolution of strength and
734 crystalline phases for alkali-activated ground blast furnace slag and fly ash-based
735 geopolymers. Cem Concr Res 2010, 40: 189-196.
736 53. Sticher H. Thermal analysis of synthetic (near-chabazite) zeolites with different Si/Al
737 ratios. Thermochim Acta 1974, 10: 305-311.
738 54. Stakebake J.L. Characterization of natural chabazite and 5A synthetic zeolites. Part 1.
739 Thermal outgassing properties. J Colloid Interf Sci 1984, 99(1): 41-49.
740 55. Mishin I.V., Piloyan G.A., Klyachko-Gurvich A.L., Rubinshtein A.M. Study of
741 decationized and dealuminized mordenites by the differential-thermal analysis method
742 and measurement of water vapour absorption. Russ Chem Bull 1973, 22(6): 1298-
743 1300.

744 56. Chandwadkar A.J., Kulkarni S.B. Thermal behaviour of modified faujasites. J
745 Thermal Anal 1980, 19: 313-320.
746 57. Kutchko B.G., Kim A.G. Fly ash characterization by SEM-EDS. Fuel 2006. 85:2537-
747 2544.
748 58. Xue Q.-F., Lu S.-G. Microstructure of ferrospheres in fly ashes: SEM, EDX and
749 ESEM analysis. J Zhejiang Univ Sci A 2008, 9(11): 1595-1600.
750 59. Zyryanov V.V., Petrov S.A., Matvienko A.A. Characterization of spinel and
751 magnetospheres of coal fly ashes collected in power plants in the former USSR. Fuel
752 2011, 90: 486-492.
753 60. Lloyd R.R., Provis J.L., van Deventer J.S.J. Microscopy and microanalysis of
754 inorganic polymer cements. 1: Remnant fly ash particles. J Mater Sci 2009, 44: 608-
755 619.
756 61. Gomes S., François M. Characterization of mullite in silicoaluminous fly ash by
757 XRD, TEM and ^{29}Si MAS NMR. Cem Concr Res 2000, 30:175-181.
758
759

760 **Table 1**. Chemical composition of the fly ash from X-ray fluorescence analysis. LOI is
761 loss on ignition at 950 ˚C

Component (weight % as oxide)	SiO_2	Al_2O_3	Fe_2O_3	CaO	MgO	SO_3	Na_2O	K_2O	LOI
Fly ash	39.00	28.01	15.43	10.27	1.50	2.00	0.71	1.38	1.69

762
763

764 **Table 2**. Chemical composition of reference silicate activators and nanosilica used to
765 prepare nanosilica/MOH activators; data provided by the suppliers

Component (weight % as oxide)	***SiO_2***	***Na_2O***	***K_2O***	***H_2O***	***Solution modulus (Ms)(SiO_2/M_2O)***
SS	28.7	8.7	-	62.4	3.30
SK	23.0	-	10.5	66.5	2.19
L300	35.7	-	-	64.3	-

766
767

768 **Table 3**. Mix description of silicate-activated fly ash binders

Properties	***Mixture ID***			
	S-Na	***S-K***	***L300-Na***	***L300-K***
alkali cation	Na^+	K^+	Na^+	K^+
silicate source	SS	SK	L300	L300
water/binder ratio	0.27	0.21	0.20	0.13

769

770

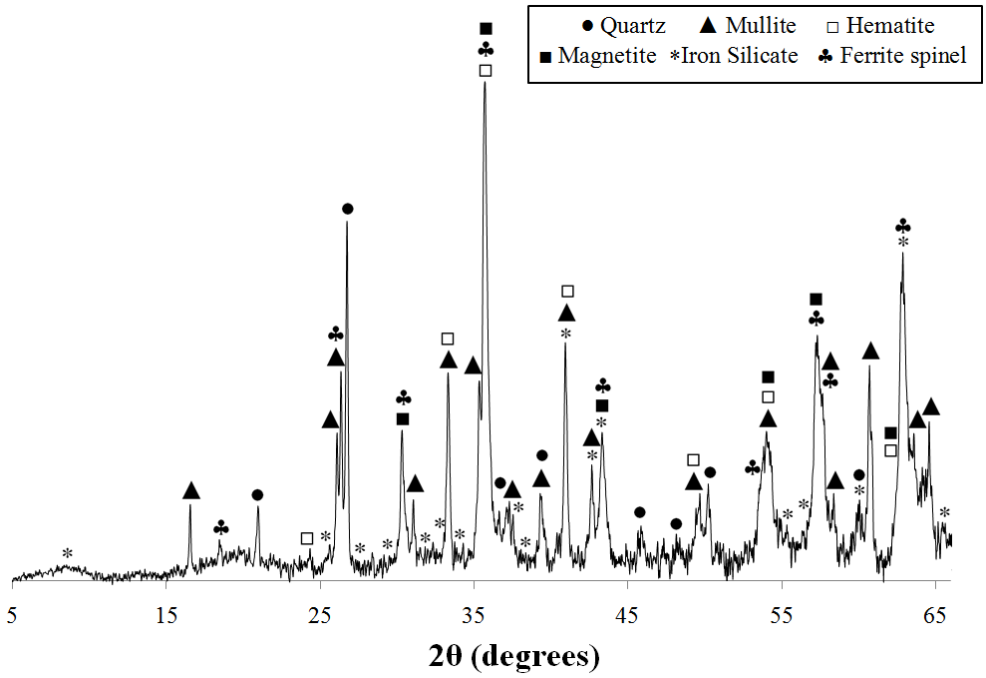

771

772 **Figure 1**. Cu-K_α diffractogram of the fly ash after mechanical treatment

773

774

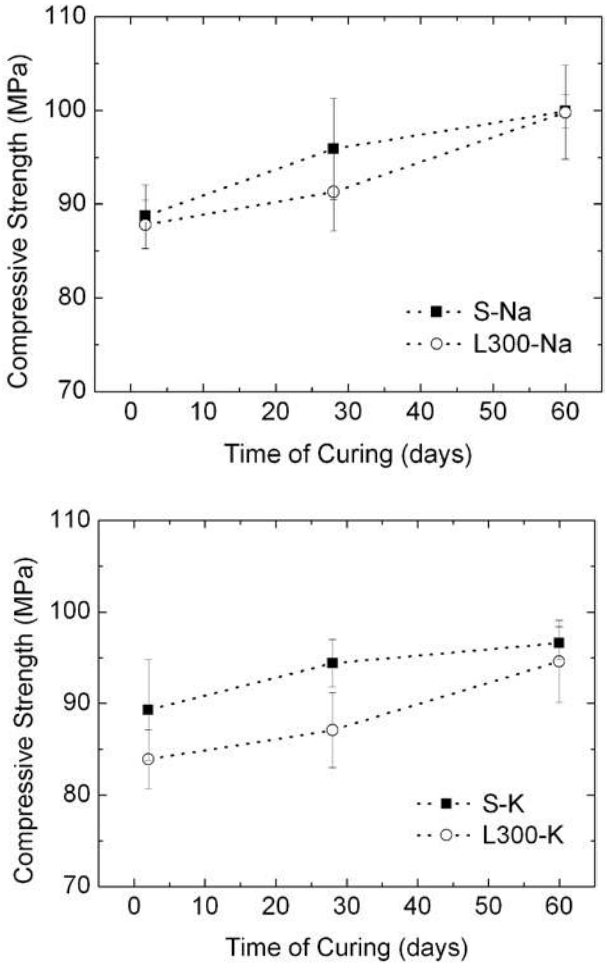

775

776 **Figure 2**. Compressive strength of alkali-activated fly ash mortars, as a function of the
777 nature of the activator. Error bars indicate one standard deviation either side of the mean.
778

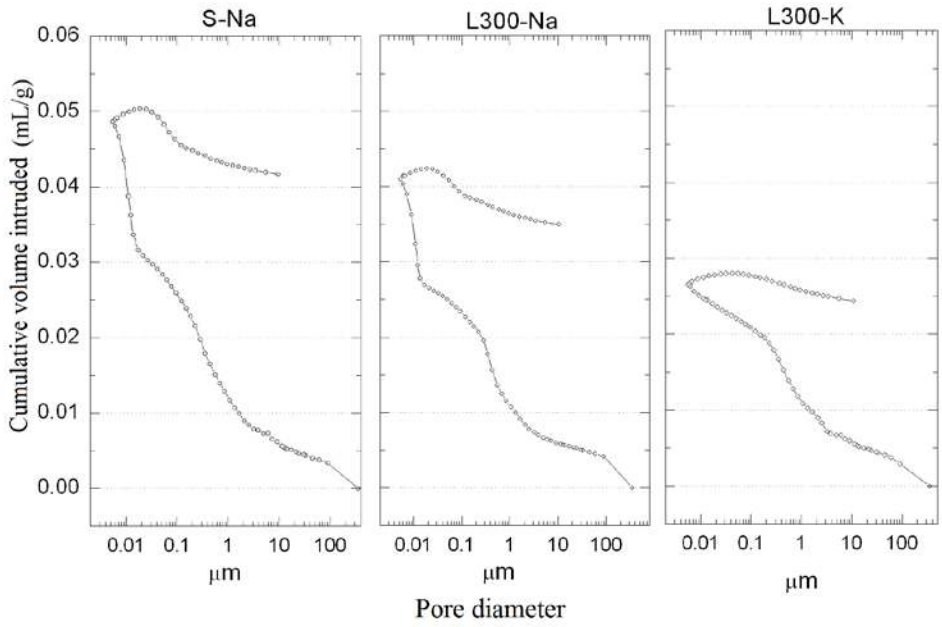

Figure 3. Cumulative volume of mercury intruded as a function of pore diameter for S-Na, L300-Na and L300-K mortars after 28 days of curing

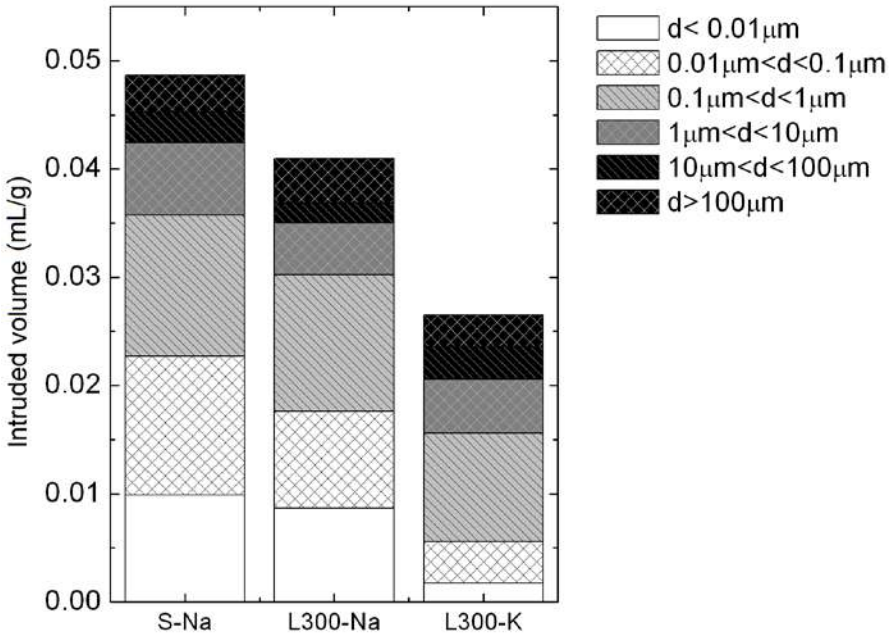

783

784 **Figure 4.** Pore size distributions obtained from mercury intrusion data for silicate-

785 activated fly ash mortars with 28 days of curing

786

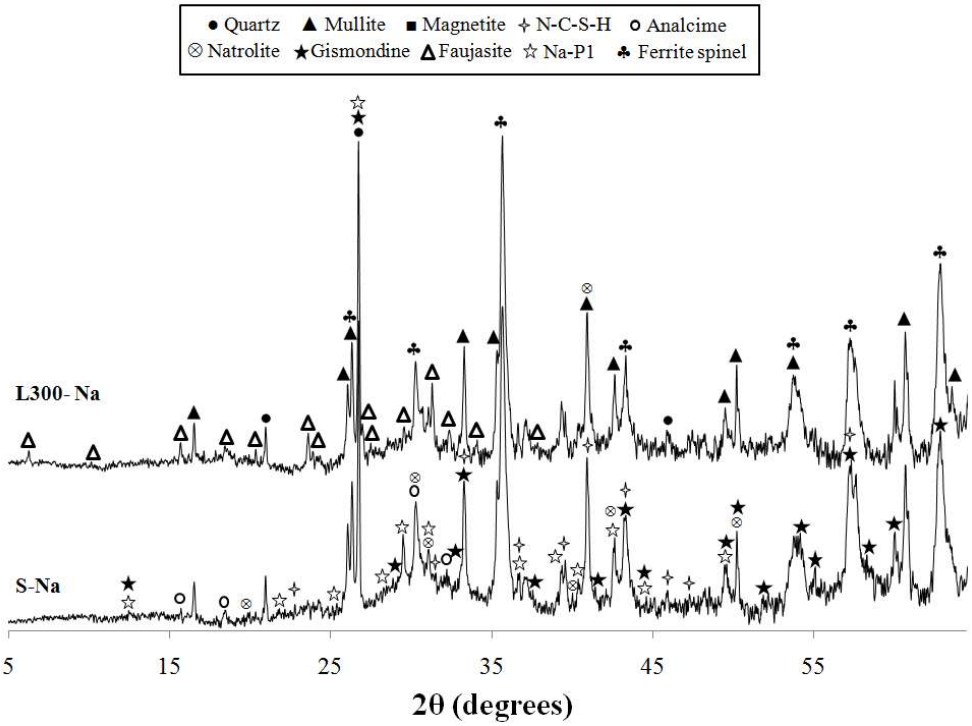

787

788 **Figure 5**. Cu-K_α diffractograms of the fly ash activated with Na-based activators. Peaks
789 present in both diffractograms are labeled in only one diffractogram for visual clarity.

790

791

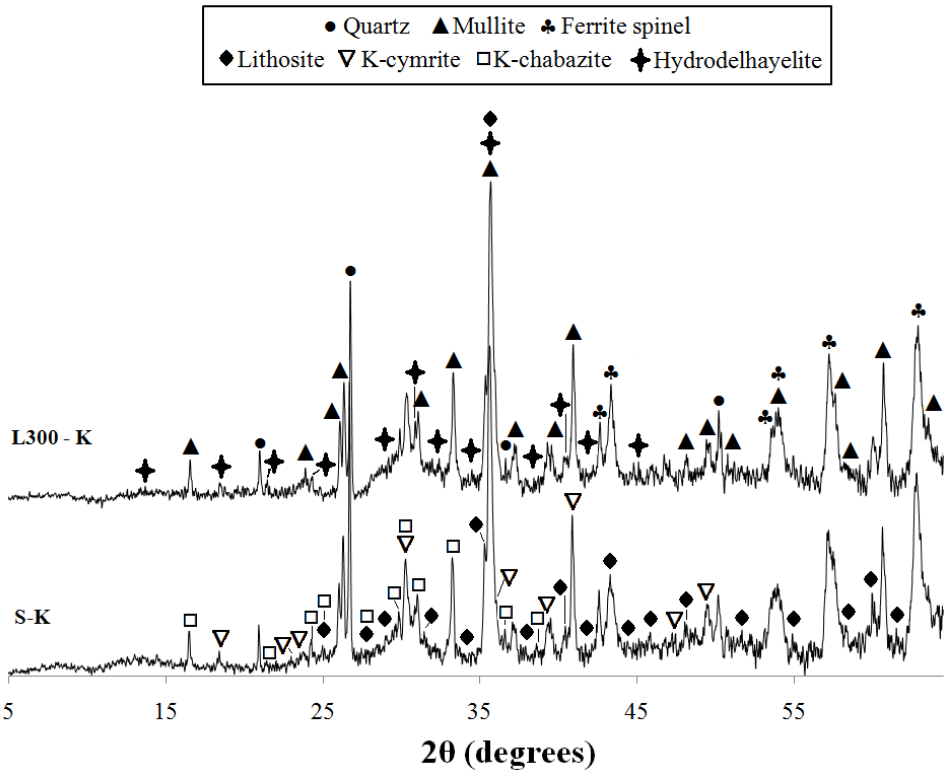

792

793 **Figure 6**. Cu-K_α diffractograms of the fly ash activated with K-based activators. Peaks
794 present in both diffractograms are labeled in only one diffractogram for visual clarity.

795

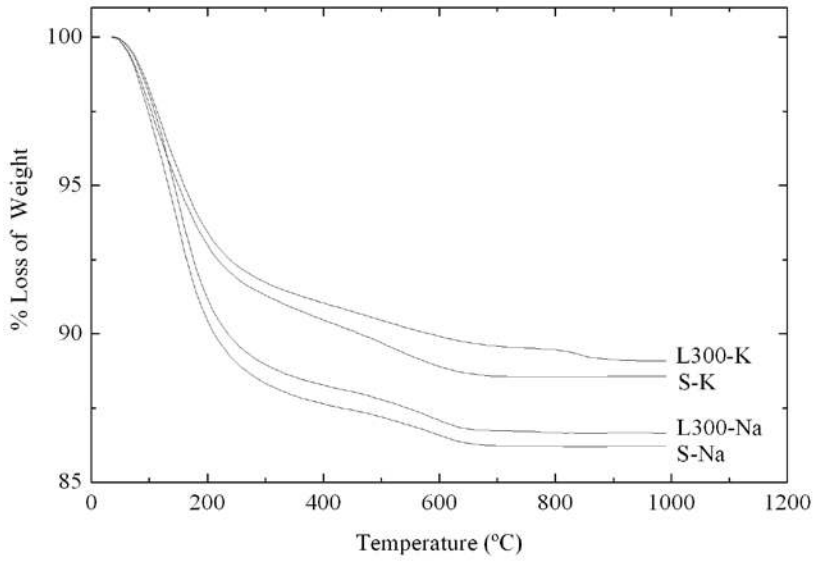

796

797 **Figure 7.** Thermograms of silicate-activated fly-ash binders at 28 days of curing

798

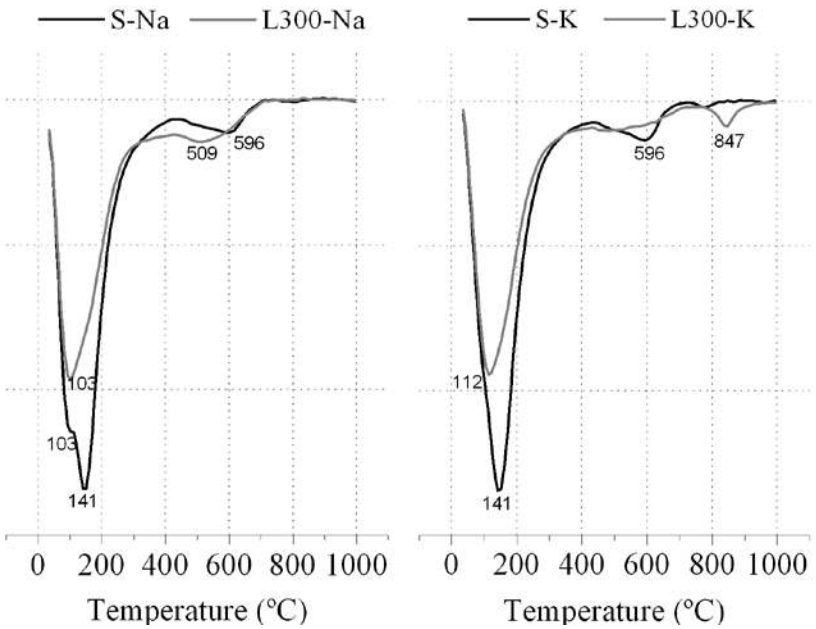

Figure 8. Differential thermograms of silicate-activated fly ash

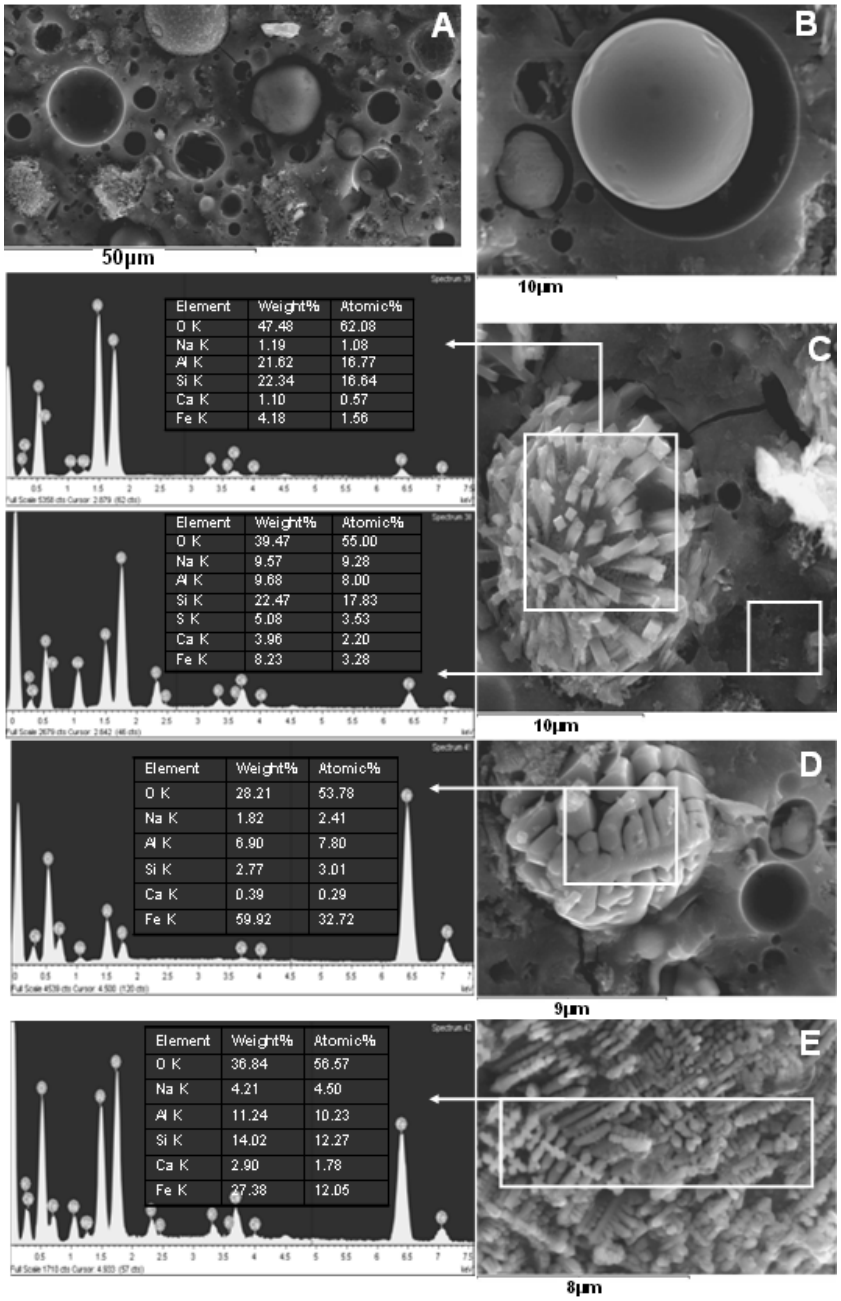

Figure 9. Scanning electron micrographs and corresponding EDS spectra of the binder activated with a commercial sodium silicate (S-Na)

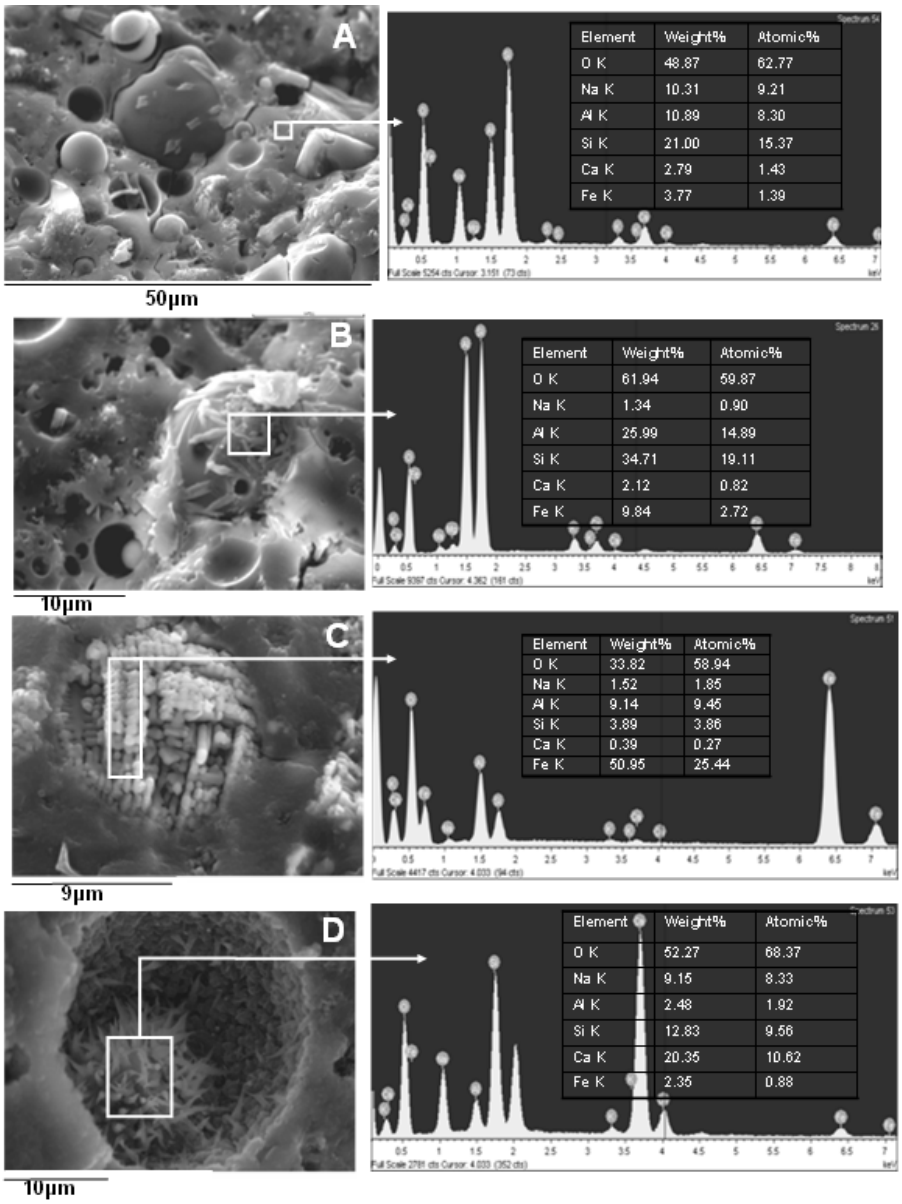

Figure 10. Scanning electron micrographs and corresponding EDS spectra for the binder activated with NaOH/nanosilica-derived activator (L300-Na)

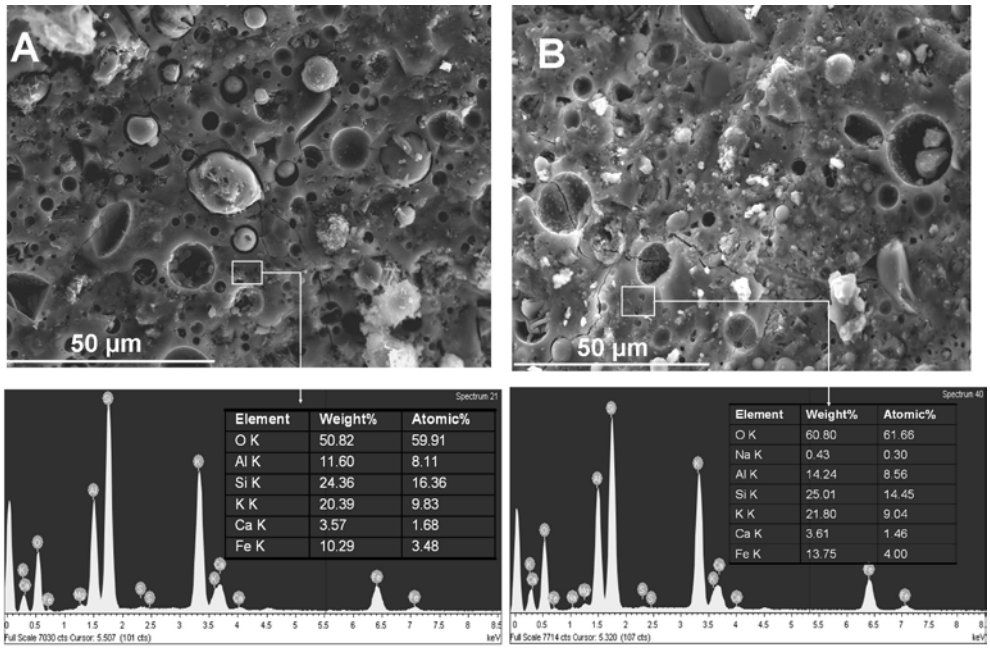

Figure 11. Scanning electron micrographs, and corresponding EDS spectra, of the binders activated with (A) commercial potassium silicate solution (S-K) and (B) KOH/nanosilica derived activator